Journal of Solid State Chemistry 246 (2017) 29–41

Contents lists available at ScienceDirect

Journal of Solid State Chemistry

journal homepage: www.elsevier.com/locate/jssc

Oxygen-storage behavior and local structure in Ti-substituted $YMnO_3$

I. Levin[a,*], V. Krayzman[a], T.A. Vanderah[a], M. Tomczyk[b], H. Wu[a], M.G. Tucker[c], H.Y. Playford[d], J.C. Woicik[a], C.L. Dennis[a], P.M. Vilarinho[b]

[a] National Institute of Standards and Technology, Gaithersburg, MD 20899, USA
[b] Department of Ceramics and Glass Engineering, University of Aveiro, Aveiro 3810-193, Portugal
[c] Spallation Neutron Source, Oak Ridge National Laboratory, Oak Ridge, TN, USA
[d] ISIS Facility, Rutherford Appleton Laboratory, Didcot, Oxford, UK

ARTICLE INFO

Keywords:
Hexagonal manganates
Oxygen storage
Redox
Diffraction
Local structure

ABSTRACT

Hexagonal manganates $RMnO_3$ (R=Y, Ho, Dy) have been recently shown to exhibit oxygen-storage capacities promising for three-way catalysts, air-separation, and related technologies. Here, we demonstrate that Ti substitution for Mn can be used to chemically tune the oxygen-breathing properties of these materials towards practical applications. Specifically, $Y(Mn_{1-x}Ti_x)O_3$ solid solutions exhibit facile oxygen absorption/desorption via reversible $Ti^{3+}\leftrightarrow Ti^{4+}$ and $Mn^{3+}\leftrightarrow Mn^{4+}$ reactions already in ambient air at ≈400 °C and ≈250 °C, respectively. On cooling, the oxidation of both cations is accompanied by oxygen uptake yielding a formula $YMn^{3+}{}_{1-x-y}Mn^{4+}{}_{y}Ti^{4+}{}_{x}O_{3+\delta}$. The presence of Ti promotes the oxidation of Mn^{3+} to Mn^{4+}, which is almost negligible for $YMnO_3$ in air, thereby increasing the uptake of oxygen beyond that required for a given Ti^{4+} concentration. The reversibility of the redox reactions is limited by sluggish kinetics; however, the oxidation process continues, if slowly, even at room temperature. The extra oxygen atoms are accommodated by the large interstices within a triangular lattice formed by the $[MnO_5]$ trigonal bipyramids. According to bond distances from Rietveld refinements using the neutron diffraction data, the $YMnO_3$ structure features under-bonded Mn and even more severely under-bonded oxygen atoms that form the trigonal bases of the $[MnO_5]$ bipyramids. The tensile bond strain around the 5-fold coordinated Mn site and the strong preference of Ti^{4+}(and Mn^{4+}) for higher coordination numbers likely provide driving forces for the oxidation reaction. Reverse Monte Carlo refinements of the local atomic displacements using neutron total scattering revealed how the excess oxygen atoms are accommodated in the structure by correlated local displacements of the host atoms. Large displacements of the under-bonded host oxygen atoms play a key part in this lattice-relaxation process, facilitating reversible exchange of significant amounts of oxygen with atmosphere.

1. Introduction

$YMnO_3$, which crystallizes with a hexagonal structure [1], has been studied extensively as an example of a non-perovskite multiferroic [e.g., 2–8]. This structure consists of layers of vertex-sharing trigonal $[MnO_5]$ bi-pyramids linked by layers of 8-fold coordinated Y^{3+} ions (Fig. 1). On cooling, at T≈1000 °C, $YMnO_3$ undergoes a phase transition from the high-temperature *P6₃/mmc* form to the non-centrosymmetric *P6₃cm* polymorph, manifested in rotations of $[MnO_5]$ polyhedra with concurrent ferrielectric-like Y displacements along the *c*-axis [7]. The effective coordination of Y changes from 8-fold to (7+1)-fold because of the strong off-centering of Y atoms within the -O-Y-O- chains along the *c*-axis. The transition is accompanied by loss of the inversion center and tripling of the unit-cell volume. Despite numerous experimental and theoretical studies [2–8], the exact origin of ferroelectricity and even the actual Curie temperature in this compound remain debatable.

The point defect chemistry in $YMnO_3$ is also somewhat uncertain. Two conflicting scenarios that propose mixed 3+/2+ [9] and 3+/4+ [10] oxidation states for Mn, respectively, have been proposed from the variable-temperature dielectric and electrical-conductivity studies. Thermal gravimetric analysis (TGA) revealed that $YMnO_3$ remains nearly stoichiometric if heat-treated in air but undergoes oxidation to $YMnO_{3+\delta}$ with δ=0.13, upon thermal cycling in oxygen [11–13]. The oxidation occurs between 300 °C and 200 °C. A much larger oxygen excess, δ=0.38, has been achieved using an oxygen pressure of 190 bar [11]. Similar behavior was reported for a series of hexagonal $RMnO_3$ (R=Ho, Er, Dy, Y) compounds [12,13]. For a given set of conditions, the amount of excess oxygen increased markedly with increasing ionic radius of the R species. The largest value of oxygen-storage capacity

---

[*] Corresponding author.
E-mail address: igor.levin@nist.gov (I. Levin).

http://dx.doi.org/10.1016/j.jssc.2016.10.029
Received 16 September 2016; Received in revised form 26 October 2016; Accepted 27 October 2016

0022-4596/

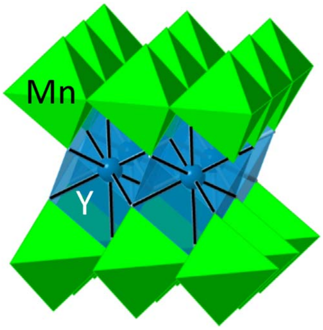

Fig. 1. Crystal structure of hexagonal $YMnO_3$ structure (space group *P6₃cm*). The Mn- and Y-centered polyhedra are indicated using green and blue colors, respectively. (For interpretation of the references to color in this figure legend, the reader is referred to the web version of this article).

reported for the $RMnO_3$ materials under 1 bar oxygen pressure is ≈1200 μmol·O/g at ≈350 °C [11], which, combined with relatively low oxygen absorption/desorption temperatures, renders them potentially viable for air-separation and related applications. Reportedly [12], the *$P6_3cm$* structure is preserved for $\delta < 0.13$, while for higher oxygen content the symmetry is reduced first to trigonal *R3c* (e.g., $\delta \approx 0.28$) and then to orthorhombic *$Pca2_1$* (e.g., $\delta = 0.4$). All these structures can be derived from the archetypical *$P6_3/mmc$* symmetry by imposing different patterns of rotations for the $[MnO_5]$ bipyramids in consecutive *c*-layers.

In the present work, we show that while $YMnO_3$ indeed remains mostly stoichiometric in air at least up to 1150 °C, $YMn_{1-x}Ti_xO_{3+\delta}$ solid solutions rapidly absorb atmospheric oxygen on cooling below 400 °C. This enhanced oxygen absorption relative to $YMnO_3$ is attributed to the redox reactions involving both Ti and Mn; importantly, the presence of Ti^{4+} promotes partial oxidation of Mn^{3+} to Mn^{4+}. We use neutron total scattering to establish the local structure in pure and Ti-substituted $YMnO_3$ and demonstrate how locally-correlated atomic shifts accommodate the excess oxygen atoms in the interstices of the host lattice. Our results suggest that substitutions on the Mn sites can be effective in optimizing the oxygen-storage properties of hexagonal $RMnO_3$ materials for practical use.

2. Experimental

Ceramic $YMn_{1-x}Ti_xO_3$ (x=0, 0.05, 0.125) samples were processed using conventional solid-state methods as detailed in [14]. “As-prepared” samples had been sintered in air at 1400 °C for 5 h. Previous studies of this system [14] indicated that for $x < 0.175$, the solid solutions retain the *$P6_3cm$* symmetry of the end compound [11]. Indeed, all our samples were phase pure with X-ray diffraction (XRD) patterns indexable according to the *$P6_3cm$* structure. Thus, the aliovalent substitution of Ti^{4+} for Mn^{3+} in $YMnO_3$ requires charge compensation which must occur by one or more of the following mechanisms: 1) reduction of Mn^{3+} to Mn^{2+}, 2) reduction of Ti^{4+} to Ti^{3+}, 3) addition of oxygen above 3 atoms per formula unit, and 4) formation of cation vacancies. As we show below, the structure absorbs excess oxygen to provide charge neutrality.

Thermal analyses were carried out between room temperature and 1150 °C with a TA [15] instruments SDT Q600 simultaneous TGA/DSC in platinum sample cups under flowing air or helium (100 ml/min), with heating/cooling rates of 5 °C/min and sample sizes 100–150 mg. The $YMnO_3$ sample was additionally measured in oxygen (100 ml/min).

Variable-temperature XRD was performed using a Panalytical Xpert Pro diffractometer equipped with an incident beam monochromator, a position-sensitive Pixcel detector, and an Anton Paar XRK2000 temperature stage. The sample powder was dispersed in ethanol and deposited as a thin layer on the platinum heater. The measurements were performed in air, helium, and nitrogen (1 atm).

Samples for transmission electron microscopy (TEM) were prepared either using mechanical thinning followed by conventional ion-milling until perforation or by grinding the powder in ethanol and dispersing the suspension on lacey-carbon-coated copper grids. The samples were examined in an FEI Titan TEM (300 kV) equipped with a high-angle annular dark field detector and a Gatan Enfina electron energy-loss spectrometer.

Variable field (from +5570 kA/m=70,000 Oe to −5570 kA/m and back) and temperature (from 300 to 950 K) magnetic measurements were performed on sintered pellets using a Quantum Design superconducting quantum interference device (SQUID) vibrating-sample magnetometer (VSM) equipped with a sample oven.

Neutron powder diffraction (NPD) measurements were performed for $YMnO_3$ and $YMn_{0.875}Ti_{0.125}O_3$ samples using BT-1 (constant wavelength λ=1.5405 Å) and Polaris (time of flight) instruments at NIST and ISIS, respectively. The sample powder was loaded in vanadium containers and temperature control was achieved using furnaces. The measurements with BT-1 were performed on heating (1st heating cycle) at six temperatures between 25 °C and 950 °C in vacuum. On Polaris, the sample was first measured on heating in 400 mTorr helium (this was the maximum pressure compliant with the facility's safety regulations) at a series of temperatures between 25 °C and 1000 °C, then cooled under the same atmosphere to 200 °C, and measured again upon heating in vacuum [16] between 200 °C and 600 °C.

X-ray absorption fine structure (XAFS) was measured for the Mn K-edge in $YMnO_3$ and $YMn_{0.875}Ti_{0.125}O_3$ samples using the NIST X23A2 beamline at the National Synchrotron Light Source. The measurements were performed in transmission. Temperature control was achieved using the Linkam THMS600 stage. Transmission data for a Mn foil positioned downstream from the sample was recorded simultaneously with each scan for energy calibration. XAFS data were processed using the Athena software [17].

Rietveld refinements using the XRD data and NPD data were performed in GSAS. Neutron total scattering patterns were processed in GUDRUN to obtain the scattering $S(Q)$ and pair-distribution $G(r)$ functions ($Q_{max} \approx 30$ Å^{-1} was used in the Fourier transform). The $G(r)$ was initially analyzed using a crystallographic Rietveld-derived model in the PDFGUI software [18]. Structural refinements using S(Q), G(r), and neutron Bragg profile were performed in RMCProfile [19]. An atomic configuration contained 11×11×6 unit cells with a total of 21,780 atoms. For each structure, the refinements were repeated five times and the structural characteristics of interest were obtained by averaging over the five refined configurations, which represent equivalent but different snapshots of the atomic arrangements.

3. Results and discussion

3.1. Thermal analysis: oxygen absorption/desorption

$YMnO_3$ exhibits a barely detectable change in mass at ≈250 °C upon thermal cycling in air (Fig. 2a). This change, which becomes more noticeable in oxygen, has been attributed to partial oxidation of Mn^{3+} to Mn^{4+}(on cooling) yielding excess oxygen in the sample with a charge-compensated formula $YMnO_{3+\delta}$ [11–13]. The loss of this small amount of excess oxygen was observed between 250 °C and 300 °C in the TGA of $YMnO_3$ under helium. (These measurements additionally ruled out the presence of any significant amount of Mn^{2+}, in accord with the behavior of the lattice parameters presented in the next section.) The behavior of $YMn_{0.875}Ti_{0.125}O_{3+\delta}$ is markedly different. In air (Fig. 2b), the first heating cycle was consistently unique with the onset of an endothermic effect near 350 °C accompanied first by a slight gain in mass followed by a significant mass loss just near 400 °C; after cooling, an overall 0.3–0.4% mass loss was observed. At high